# Supplementary Materials for

# Generation of photonic spin-controlled accelerating light beams along arbitrary curved trajectories

**SI: Derivation of the Jones matrix $J$ and its eigenvalues and eigenvectors.**

Assuming input polarization states $\{|\alpha^+\rangle, |\alpha^-\rangle\}$ upon which the metasurface should impart two independent phase profiles, $\varphi_1(x,y)$ and $\varphi_2(x,y)$, be given by orthogonal polarization states $|\alpha^+\rangle = \begin{bmatrix}\alpha_1^+\\ \alpha_2^+\end{bmatrix}$ and $|\alpha^-\rangle = \begin{bmatrix}\alpha_1^-\\ \alpha_2^-\end{bmatrix}$. We can find a design of a linearly birefringent metasurface where the output polarization states become $\{|(\alpha^+)^*\rangle, |(\alpha^-)^*\rangle\}$; denoting complex conjugate of input polarization states. This means that they have the same states as the input states with flipped handedness. Such device can be described by Jones matrix $J(x,y)$ that simultaneously satisfies

$$J(x,y)\,|\alpha^+\rangle = e^{i\varphi_1(x,y)}|(\alpha^+)^*\rangle \tag{S1}$$

and

$$J(x,y)\,|\alpha^-\rangle = e^{i\varphi_2(x,y)}|(\alpha^-)^*\rangle \tag{S2}$$

In our design, the input polarization states are orthogonal circular polarizations states:

$$|L\rangle = \begin{bmatrix}1\\ i\end{bmatrix} \tag{S3}$$

$$|R\rangle = \begin{bmatrix}1\\ -i\end{bmatrix} \tag{S4}$$

Then, the original system can be expressed as

$$J(x,y)\begin{bmatrix}1\\ i\end{bmatrix} = e^{i\varphi_1(x,y)}\begin{bmatrix}1\\ -i\end{bmatrix} \tag{S5}$$

and

$$J(x,y)\begin{bmatrix}1\\ -i\end{bmatrix} = e^{i\varphi_2(x,y)}\begin{bmatrix}1\\ i\end{bmatrix} \tag{S6}$$

Upon matrix inversion of Eq. S5 and S6 we obtain,

$$J(x,y) = \begin{bmatrix} e^{i\varphi_1(x,y)} & e^{i\varphi_2(x,y)} \\ -ie^{i\varphi_1(x,y)} & ie^{i\varphi_2(x,y)}\end{bmatrix}\begin{bmatrix}1 & 1\\ i & -i\end{bmatrix}^{-1} \tag{S7}$$

Then, we can show that the desired matrix $J(x,y)$ is

$$J(x,y)=\frac{1}{2}\begin{bmatrix} e^{i\varphi_1(x,y)}+e^{i\varphi_2(x,y)} & ie^{i\varphi_2(x,y)}-ie^{i\varphi_1(x,y)} \\ ie^{i\varphi_2(x,y)}-ie^{i\varphi_1(x,y)} & -e^{i\varphi_1(x,y)}-e^{i\varphi_2(x,y)} \end{bmatrix} \tag{S8}$$

where $\varphi_1(x,y)$ and $\varphi_2(x,y)$ are phase profiles of arbitrary accelerating beams. This matrix provides a general form for conversion between two arbitrary accelerating beams and even arbitrary structured light. By calculating Jones matrix $J(x,y)$, we can obtain the eigenvalues as

$$\xi_1=e^{i[\frac{1}{2}(\varphi_1(x,y)+\varphi_2(x,y))]} \qquad \xi_2=e^{i[\frac{1}{2}(\varphi_1(x,y)+\varphi_2(x,y))-\pi]} \tag{S9}$$

and eigenvectors as

$$|r_1\rangle=\begin{bmatrix}\cos\frac{1}{4}[\varphi_1(x,y)-\varphi_2(x,y)]\\ sin\frac{1}{4}[\varphi_1(x,y)-\varphi_2(x,y)]\end{bmatrix} \qquad |r_2\rangle=\begin{bmatrix}-\sin\frac{1}{4}[\varphi_1(x,y)-\varphi_2(x,y)]\\ cos\frac{1}{4}[\varphi_1(x,y)-\varphi_2(x,y)]\end{bmatrix} \tag{S10}$$

Thus, the Jones matrix $J(x,y)$ can be decomposed into canonical form $J=P\Lambda P^{-1}$, where $\Lambda$ is a diagonal matrix and *P* is an invertible matrix. We can write the Jones matrix for the control and conversion between two arbitrary optical beams as

$$J(x,y)=\mathrm{P}\Lambda\mathrm{P}^{-1}=\begin{bmatrix}\cos\frac{1}{4}\left[\varphi_1(x,y)-\varphi_2(x,y)\right] & -\sin\frac{1}{4}[\varphi_1(x,y)-\varphi_2(x,y)]\\ sin\frac{1}{4}[\varphi_1(x,y)-\varphi_2(x,y)] & cos\frac{1}{4}[\varphi_1(x,y)-\varphi_2(x,y)]\end{bmatrix}\cdots$$

$$\begin{bmatrix}e^{i[\frac{1}{2}(\varphi_1(x,y)+\varphi_2(x,y))]} & 0\\ 0 & e^{i[\frac{1}{2}(\varphi_1(x,y)+\varphi_2(x,y))-\pi]}\end{bmatrix}\begin{bmatrix}\cos\frac{1}{4}\left[\varphi_1(x,y)-\varphi_2(x,y)\right] & -\sin\frac{1}{4}[\varphi_1(x,y)-\varphi_2(x,y)]\\ sin\frac{1}{4}[\varphi_1(x,y)-\varphi_2(x,y)] & cos\frac{1}{4}[\varphi_1(x,y)-\varphi_2(x,y)]\end{bmatrix} \tag{S11}$$

Since Jones matrix $J(x,y)$ works in the linear polarization basis and *P* can be regarded as a rotation matrix for the matrix $\Lambda$, we can obtain that the phase shifts are $\delta_x(x,y)=[\varphi_1(x,y)+\varphi_2(x,y)]/2$ and $\delta_y(x,y)=[\varphi_1(x,y)+\varphi_2(x,y)]/2-\pi$ and the rotation angle is $\theta(x,y)=[\varphi_1(x,y)-\varphi_2(x,y)]/4$.

## SII: Sample fabrication

500 μm-thick, double-side polished fused silica substrates were first prime-vapor-coated with a monolayer of hexamethyldisilazane (HMDS) and then spin-coated with a layer of 600 nm thick, positive-tone electron beam (e-beam) resist. Afterwards, the samples were coated with a layer of 10 nm thick Aluminum (Al) via thermal evaporation, which suppressed the charging effect during the subsequent e-beam lithography step. The e-beam lithography was performed at an accelerating voltage of 100 kV and beam current of 2 nA. The samples were developed in hexyl-acetate for 120 s. Next, the patterned samples were coated with $TiO_2$ using atomic layer deposition (ALD). The ALD was done at a low temperature of 363 K to avoid deformation of the resist pattern. After the ALD, the over-coated $TiO_2$ layer was etched by the inductively-coupled-plasma reactive ion etching (ICP-RIE), with a gas mixture of $Cl_2$ and $BCl_3$. The etching was stopped when the over-coated $TiO_2$ had been fully removed and the e-beam resist was exposed. Finally, the samples were exposed to UV irradiation, followed by soaking in n-methyl-2-pyrrolidone, which removed the resist and produced the array of $TiO_2$ nanoposts with pre-designed geometries.

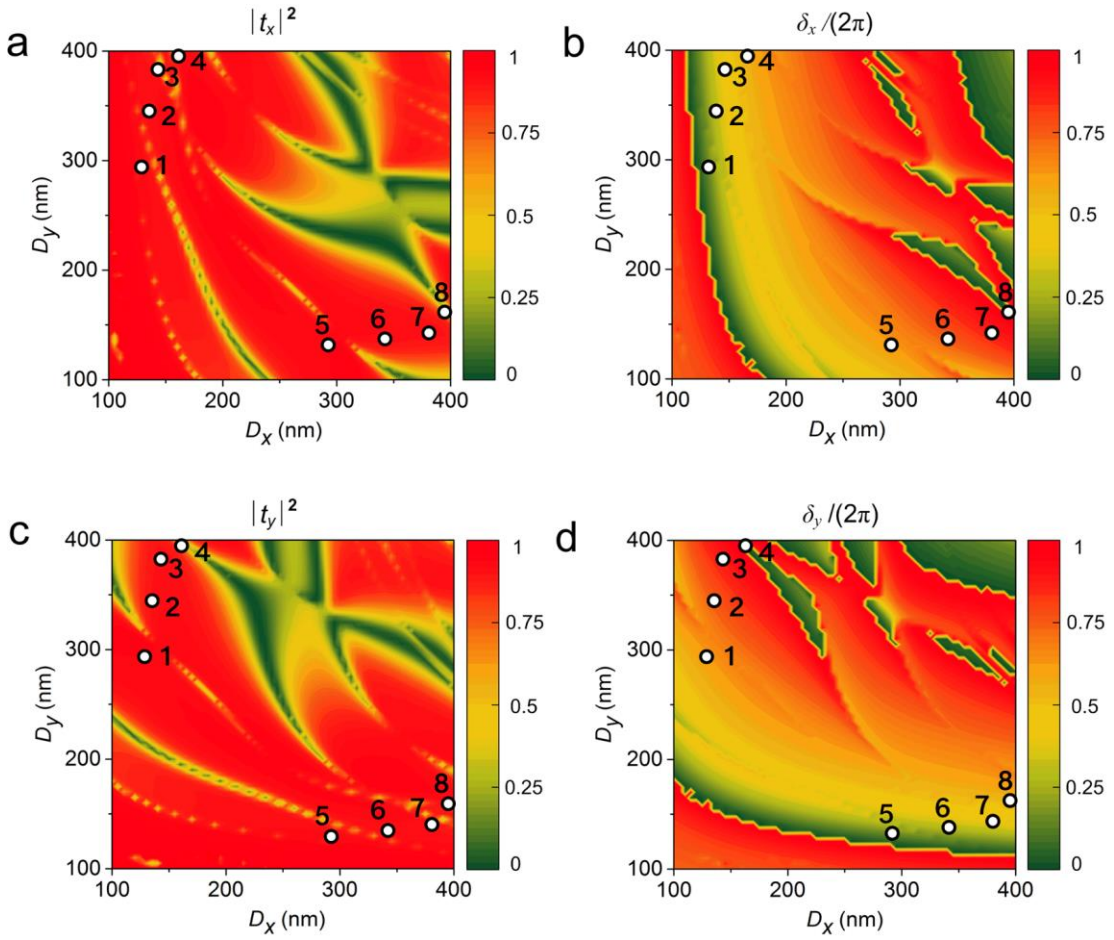


**Figure S1.** Calculated cross-polarized transmission coefficients (a. $|t_x|^2$; c. $|t_y|^2$) and phase shifts (b. $\delta_x$; d. $\delta_y$) as a function of elliptical nanopost diameters ($D_x$, $D_y$) at the wavelength of 532 nm. The chosen structural parameters (white dots) for four fundamental nanopost structures is nanopost #1: $D_x$=130 nm, $D_y$= 295 nm; nanopost #2: $D_x$=135 nm, $D_y$= 345 nm; nanopost #3: $D_x$=140 nm, $D_y$= 385 nm; nanopost #4: $D_x$=160 nm, $D_y$= 395 nm. The other four mirror structures #5 ~ #8 can be obtained just by switching $D_x$ and $D_y$ on nanopost #1-4.

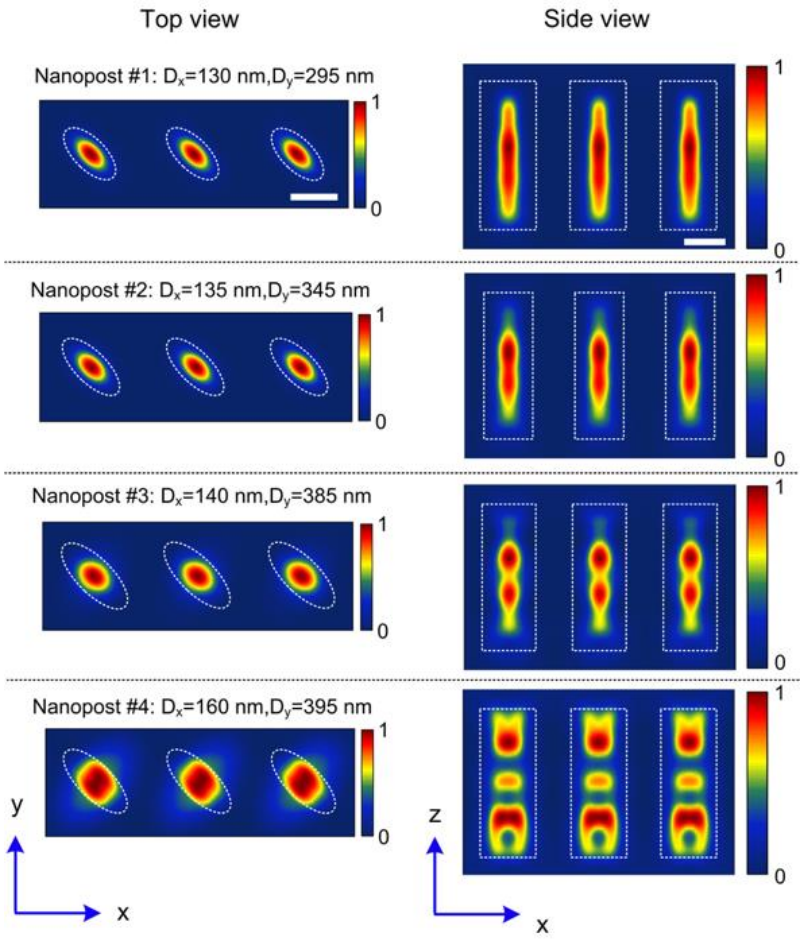


**Figure S2.** Top views (left: *xy* cross-section) and side views (right: *xz* cross-section) of the normalized magnetic field intensity in a periodic array for different nanopost structures. The array of nanoposts are rotated by 45° with respect to the square lattice. A plane wave with *y*-polarization is normally incident on the $TiO_2$ nanoposts from the substrate side. The boundaries of the nanoposts are depicted by dashed white lines. Scale bars represent 200 nm in all directions.

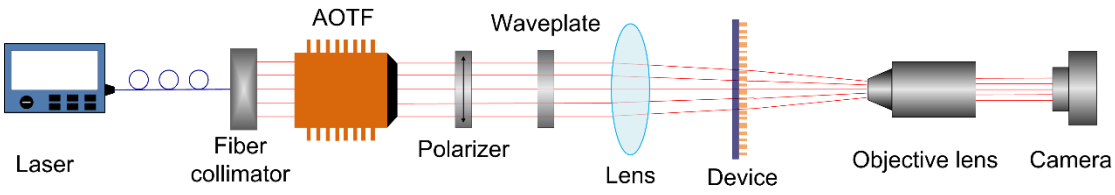


**Figure S3.** Schematic illustration of the measurement setup used for characterization of metasurface devices generating switchable accelerating light beams. The quarter-wave plate (QWP) is rotated to convert the polarization of incident light from LCP to RCP. AOTF: Acousto-Optic Tunable Filter system.

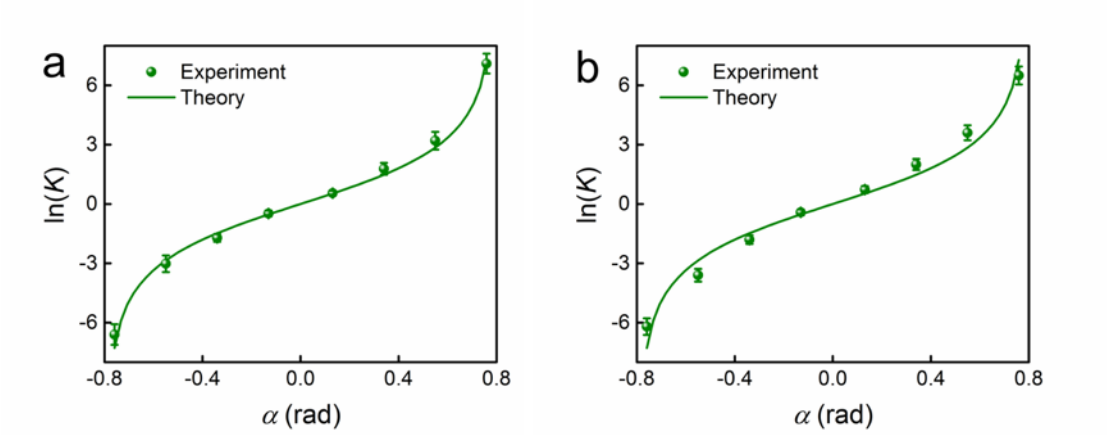


**Figure S4.** Calculated and measured intensity ratio $K$ (in logarithmic scale) between $|R\rangle|A_r\rangle$ and $|L\rangle|A_l\rangle$ as a function of the QWP rotation angle α for the metasurface devices generating (a) two Airy beams and (b) biquadratic and natural logarithm beams. The uncertainties are one standard deviation of deflection distance for repeated experimental measurements (four in total).

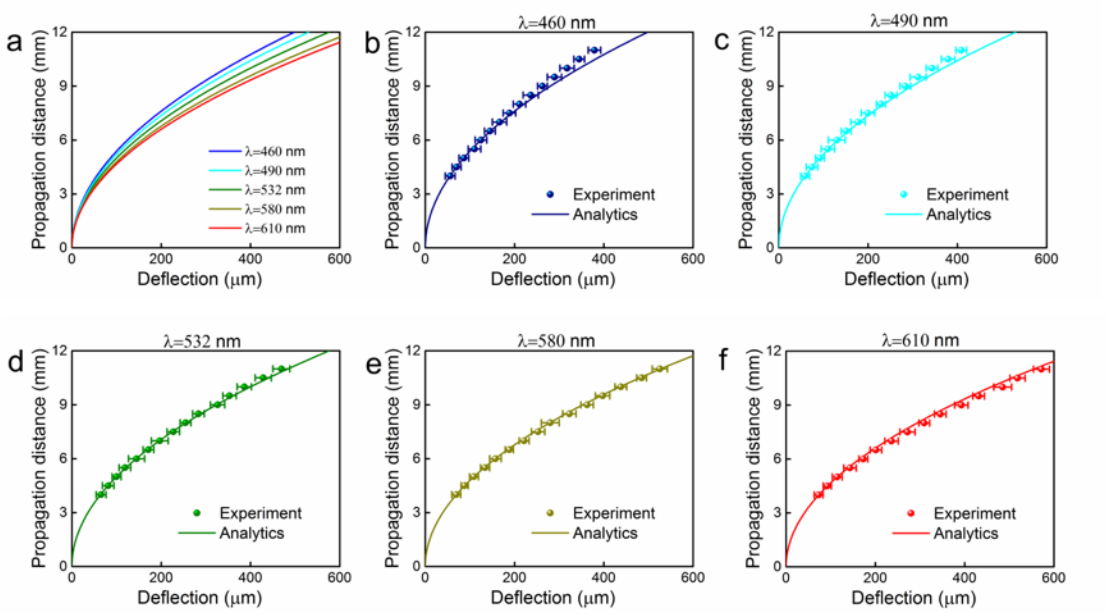


**Figure S5.** (a) Calculated propagation trajectories of the metasurface-generated Airy beams under the illumination at different wavelengths. (b)-(f) Experimentally measured propagation trajectories of Airy beams at different wavelengths. The uncertainties are one standard deviation of deflection distance for repeated experimental measurements (four in total).

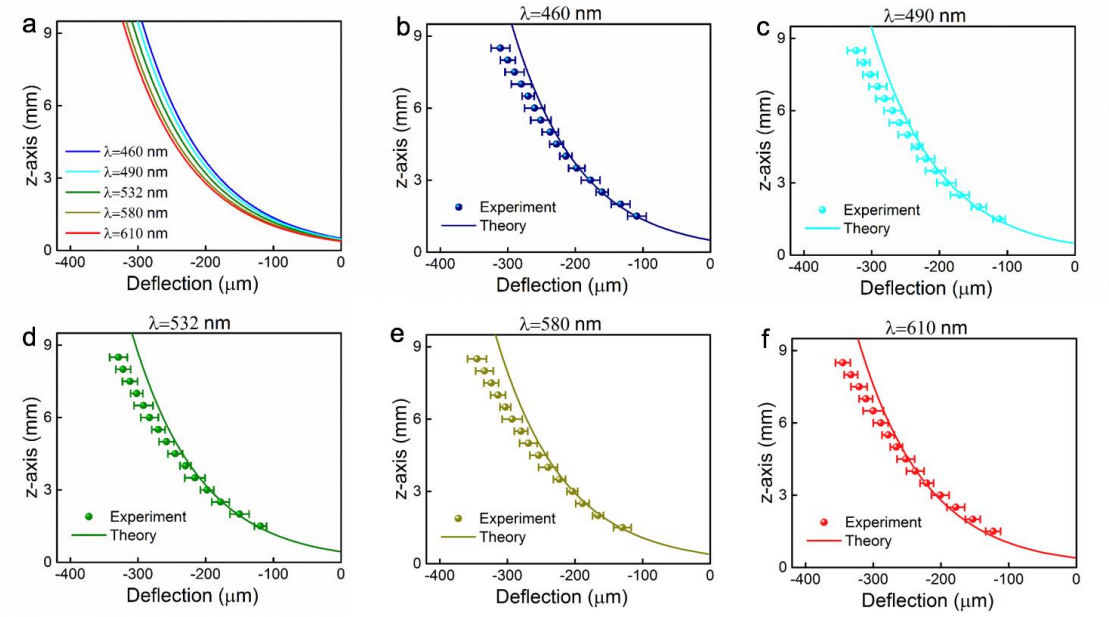


**Figure S6.** (a) Calculated propagation trajectories of the metasurface-generated accelerating beam following natural logarithm caustic trajectories under the illumination at different wavelengths. (b)-(f) Experimentally measured propagation trajectories of accelerating beams at different wavelengths. The uncertainties are one standard deviation of deflection distance for repeated experimental measurements (four in total).

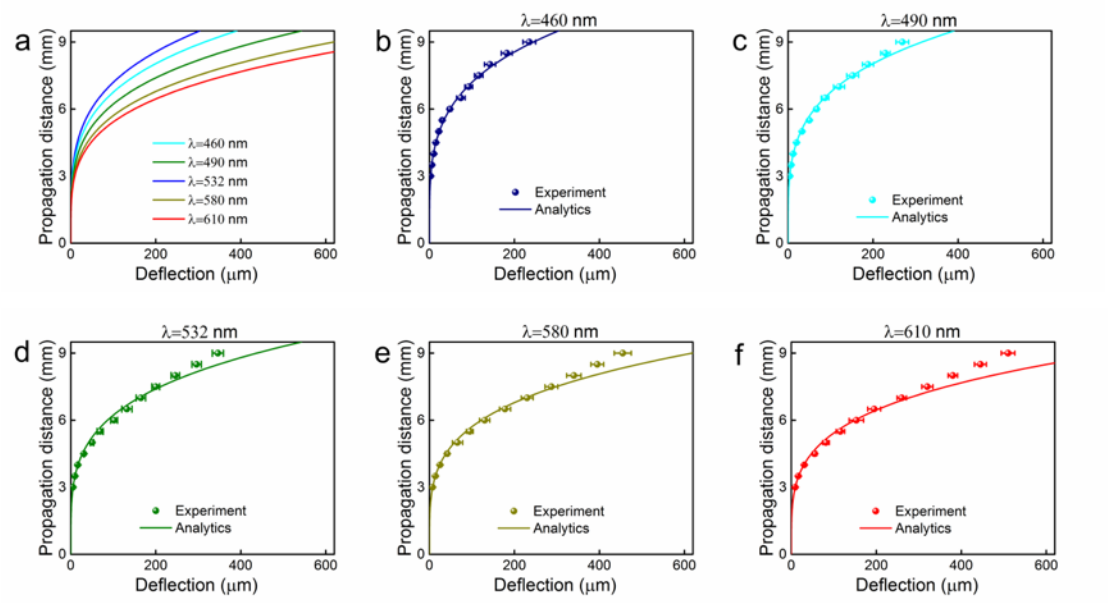


**Figure S7.** (a) Calculated propagation trajectories of the metasurface-generated accelerating beam following biquadratic caustic trajectories under the illumination at different wavelengths. (b)-(f) Experimentally measured propagation trajectories of accelerating beams at different wavelengths. The uncertainties are one standard deviation of deflection distance for repeated experimental measurements (four in total).

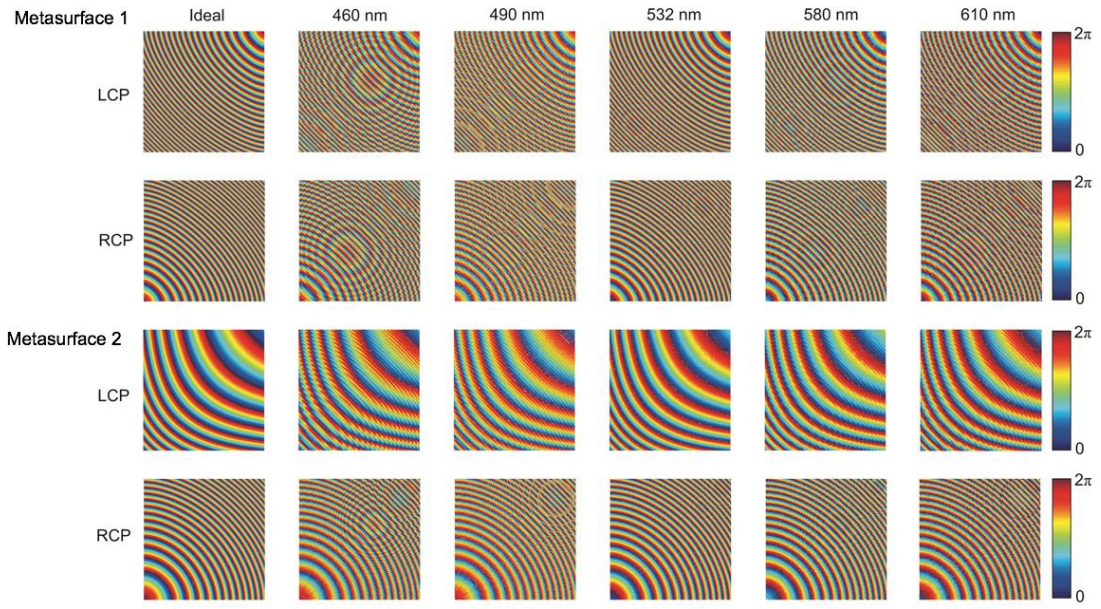


**Figure S8.** The calculated phase profiles of two metasurfaces for LCP and RCP light at multiple wavelengths. The horizontal and vertical axes of each subplot represent a spatial area of 450 μm × 450 μm of the fabricated metasurface samples 1 & 2. The color scales represent the phase profiles of the metasurfaces measured in Figure 3 & 4, which are designed to achieve the generation and switching between two arbitrary accelerating light beams to follow different caustic trajectories in free-space. As shown in this figure, the phase profiles of this $TiO_2$ metasurface are very similar for the selected multi-wavelengths.